Human Molecular Genetics, 2018, Vol. 27, No. 17 2986–3001

doi: 10.1093/hmg/ddy190
Advance Access Publication Date: 22 May 2018
Original Article

ORIGINAL ARTICLE

The presenilin loop region is essential for glycogen synthase kinase 3 β (GSK3β) mediated functions on motor proteins during axonal transport

Rupkatha Banerjee, Zoe Rudloff, Crystal Naylor, Michael C. Yu and Shermali Gunawardena*

Department of Biological Sciences, The State University of New York at Buffalo, Buffalo, NY 14260, USA

*To whom correspondence should be addressed at: Department of Biological Sciences, The State University of New York at Buffalo, 109 Cooke Hall, North/Amherst Campus, Buffalo, NY 14260, USA. Tel: +1 7166454915; Fax: +1 7166452975; Email: sg99@buffalo.edu

Abstract

Neurons require intracellular transport of essential components for function and viability and defects in transport has been implicated in many neurodegenerative diseases including Alzheimer's disease (AD). One possible mechanism by which transport defects could occur is by improper regulation of molecular motors. Previous work showed that reduction of presenilin (PS) or glycogen synthase kinase 3 beta (GSK3β) stimulated amyloid precursor protein vesicle motility. Excess GSK3β caused transport defects and increased motor binding to membranes, while reduction of PS decreased active GSK3β and motor binding to membranes. Here, we report that functional PS and the catalytic loop region of PS is essential for the rescue of GSK3β-mediated axonal transport defects. Disruption of PS loop (PSΔE9) or expression of the non-functional PS variant, PSD447A, failed to rescue axonal blockages *in vivo*. Further, active GSK3β associated with and phosphorylated kinesin-1 *in vitro*. Our observations together with previous work that showed that the loop region of PS interacts with GSK3β propose a scaffolding mechanism for PS in which the loop region sequesters GSK3β away from motors for the proper regulation of motor function. These findings are important to uncouple the complex regulatory mechanisms that likely exist for motor activity during axonal transport *in vivo*.

Introduction

Presenilin (PS) is an evolutionarily conserved, multipass transmembrane (TM) protein (1) with a single large hydrophilic loop between TM domains 6 and 7 (2,3). PS is essential for development as knockout of PS in mice (4–6) and flies (7,8) are lethal. PS has been implicated in multiple physiological roles, such as calcium homeostasis (9), membrane trafficking (10) and cell–cell adhesion (11). In mammals, PS exists as two homologs (PS1 and PS2) which share 67% similarity and are redundant in their functions (12–15) but only a single PS homolog is present in *Drosophila* (16,17). However, in *Drosophila*, PS undergoes alternative splicing (17), generating two isoforms (PS+14 and PS−14) that differ with respect to a 14 amino acid insertion in the hydrophilic loop domain, but show functional similarity (18).

PS undergoes endoproteolytic processing within the exon-9 region of the hydrophilic loop resulting in N- and C-terminal fragments (19). Two conserved aspartate residues, Asp 257 in TM6 and Asp 385 in TM7, are critical for endoproteolysis of PS (13). Endoproteolysis is essential for PS's 'presenilase' function, defined by the ability to act as an autoactivated intramembranous aspartyl protease (13,20), identified by the lack of presenilase inhibition by several potent γ-secretase inhibitors (21); and

Received: January 26, 2018. **Revised:** May 2, 2018. **Accepted:** May 10, 2018

© The Author(s) 2018. Published by Oxford University Press. All rights reserved.
For permissions, please email: journals.permissions@oup.com

for its γ-secretase function, identified by intramembrane cleavage of the TM protein amyloid precursor protein (APP) (22,23). Further, autoproteolysis of PS was proposed to cause conformational changes to the loop domains of PS (24). Modeling analysis has shown that conformational changes critical for the maturation of PS activity within the exon 9 loop directly controls access to a channel-like interior and to the catalytic site (25,26), demonstrating the complexity of PS function.

Over 150 mutations in PS contribute to early-onset familial Alzheimer's disease (FAD) but it is unclear whether these PS mutations contribute to a gain of function (6,27) or a loss of function disease mechanism (28,29). The FAD PSΔE9 mutation results in the deletion of exon 9, encoding part of the hydrophilic loop (30). Although this mutation fails to undergo endoproteolytic cleavage in mice (31) and in cells (19), normal γ-secretase activity was seen as APP and Notch were cleaved in mammalian cells (13,19). However, γ-secretase activity was reduced in isogenic human PSΔE9 patient stem cells (27). FAD mutations PS D257A and PS D385A carry amino acid substitutions at the two conserved aspartate residues within TM6 and TM7, and mimic non-functional PS or a PS-null state with no endoproteolysis (13) with diminished γ-secretase cleavage of APP in mammalian cells (13,32). A similar effect was observed when an aspartate residue in PS2 was mutated (D366A) (14). γ-secretase activity was completely abolished when aspartate residues in both PS1 and PS2 were mutated (33). Additionally, PS D257A and PS D385A mutations prevent Notch cleavage (34), however, the trafficking of Notch to the plasma membrane was unaffected (32,35,36). In addition to the γ-secretase function, studies have shown that PS also has a scaffolding role to facilitate β-catenin phosphorylation by protein kinase A (PKA) and glycogen synthase kinase 3 beta (GSK3β) (37) and for its turnover (38–40). In this context, amino acids 250–298 interacts with GSK3β (41,42) and amino acids 299–427 binds β-catenin (37), bringing GSK3β to β-catenin for its phosphorylation (43). Deletion of the loop region, including the GSK3β binding site (41) in the PSΔE9 mutant showed reduced affinity for GSK3β and slowed the rate of β-catenin turnover (39). Work has also shown that phosphorylation of serine 353 and 357 of PS by GSK3β induces a structural change in the hydrophilic loop of PS, which reduced the interaction of β-catenin and decreased its turnover (43). Although it is unclear how a scaffolding function for PS contributes to AD, the FAD PSΔE9 mutant showed increased Aβ production (23,44).

Studies have shown that PS has a role during axonal transport. PS moves bidirectionally within both peripheral nervous system (PNS) (45,46) and central nervous system axons (47) and was proposed to be present with APP containing axonal vesicles (48). Consistent with this, genetic reduction of PS in *Drosophila* larval nerves stimulated both the anterograde and retrograde velocities of APP vesicles but not synaptotagmin (SYNT) vesicles (49). Strikingly, a similar phenotype was observed with genetic reduction of GSK3β in *Drosophila* (50). Although biochemical associations between PS and GSK3β have been observed (39,41), we previously showed a functional interaction between PS and GSK3β in the context of axonal transport (51). Although homozygous PS or GSK3β loss of function mutants are lethal, larvae heterozygous for both PS and GSK3β show a paralytic crawling phenotype and do not eclose to adults (51). These larvae also contained axonal blockages at levels comparable to homozygous loss of function motor protein mutants (52). Intriguingly, heterozygous PS mutants showed decreased active GSK3β on membranes together with decreased kinesin and dynein binding to membranes, similar to heterozygous GSK3β mutants. Together, these observations suggest that PS and GSK3β are functionally coupled during axonal transport. Since *in vitro* work in cells has suggested that GSK3β can phosphorylate kinesin light chain (KLC), releasing kinesin from vesicles (53), perhaps PS is involved in controlling GSK3β-mediated roles on motor proteins during axonal transport. Since the hydrophilic loop region of PS binds GSK3β (41) perhaps PS loop is essential for these GSK3β-mediated roles on axonal transport. Alternatively, since PS was shown to be an unprimed substrate of GSK3β (54) and that GSK3β activity modified the localization and function of PS (55), perhaps GSK3β is involved in PS-mediated roles during axonal transport. Here, we test these predictions using *Drosophila* genetics, biochemical analysis and *in vivo* imaging. Our observations show that an intact loop region and functional PS is essential for proper axonal transport. Our results propose a model in which the hydrophilic PS loop region sequesters GSK3β away from motors likely for the proper regulation of motor function during axonal transport *in vivo*.

Results

Functional PS is required to rescue GSK3β-mediated axonal transport defects

One prediction of the hypothesis that PS and GSK3β are functionally coupled during axonal transport is that functional PS is required for GSK3β-mediated roles during axonal transport. Previously, we showed that expression of the *Drosophila* homolog of GSK3β, Shaggy (SGG), in all neurons using the APPL-GAL4 driver caused axonal blockages compared with wild-type (WT) (51) (Fig. 1A–C). Larval segmental nerves from larvae expressing SGG^{WT} contained accumulations of the synaptic vesicle protein cysteine string protein (CSP), similar to what was observed in larvae containing loss of function mutations of genes encoding motor proteins (56–58). These accumulations are called axonal blockages and are observed both in fixed (51,52,56,58–62) or live larval segmental nerves (52,60,61,63–65) and has been used to successfully identify novel genes involved in axonal transport (58,61,62,64,66). Under electron microscopy, many types of identifiable axonal cargo (mitochondria, dense core vesicles) are observed within these axonal blockages (49,57,58). In contrast to larvae expressing GSK3β/SGG, expression of *Drosophila* PS (PS+14 or PS−14) in all neurons did not show axonal blockages but showed smooth CSP staining, similar to what is observed in segmental nerves from WT larvae (Fig. 1A and D, Supplementary Material, Fig. S1C). To test that functional PS is required for GSK3β-mediated roles, we generated larvae expressing both SGG^{WT} and PS. As a control, we also generated larvae expressing both SGG^{WT} and GFP (UAS-EGFP). Strikingly, we observed that larvae expressing both SGG^{WT} and PS+14 showed smooth CSP stained segmental nerves (Fig. 1E). Note that larvae expressing SGG^{WT} and GFP show axonal blockages at similar levels to larvae expressing SGG^{WT} alone (Fig. 1J), indicating that the rescue we observe is specific and is not due to competing events for two transgenes within one organism. Excess PS also rescued axonal blockages seen in larvae expressing SGG^{ACTIVE} alone. Larvae expressing both SGG^{ACTIVE} and PS+14 or PS−14, also contained smooth CSP stained segmental nerves (Fig. 1F, Supplementary Material, Fig. S1). Quantification analysis of the average number of axonal blockages per larvae indicated that the extent of blockages seen in larvae expressing SGG^{WT} ($P < 0.05$) or SGG^{ACTIVE} ($P < 0.05$) alone was significantly rescued with the expression of PS (Fig. 1H and I, Supplementary Material, Fig. S1I). These observations are in contrast to our previous work that showed that larvae expressing GSK3β/SGG in the context of 50% reduction of PS

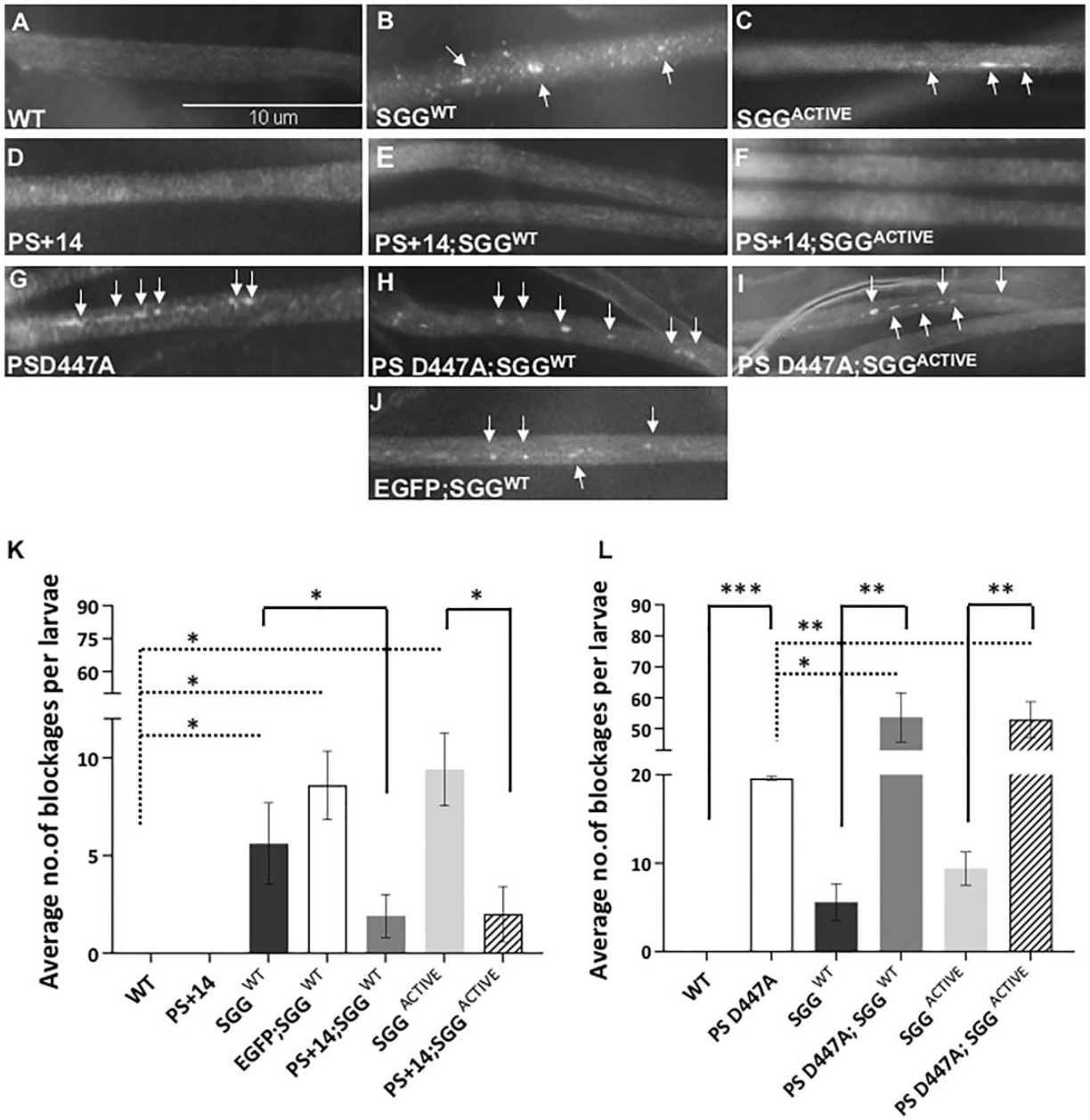

Figure 1. Expression of functional PS rescues GSK3β-mediated axonal transport defects. (**A**) A representative larval segmental nerve from WT larva stained with the synaptic vesicle marker Cysteine string protein (CSP) shows smooth staining in their larval nerves. Scale Bar = 10 μm. (**B** and **C**) In contrast, larval segmental nerves expressing SGG^{WT} or SGG^{ACTIVE} show axonal blockages (arrows) that stain with CSP. (**D**) Larval segmental nerves from larvae expressing full-length *Drosophila* PS (PS+14) show smooth CSP stained larval nerves. (**E**) Larval segmental nerves from larvae expressing PS+14 and SGG^{WT} show smooth CSP staining. (**F**) Larval segmental nerves from larvae expressing PS+14 and SGG^{ACTIVE} also show smooth CSP staining. (**G**) Larvae expressing a non-functional form of PS, PSD447A show axonal blockages (arrows). (**H**) Larval segmental nerves from larvae expressing PSD447A and SGG^{WT} show axonal blockages (arrows). (**I**) Larvae expressing PSD447A and SGG^{ACTIVE} also show axonal blockages (arrows). (**J**) Larvae expressing SGG^{WT} and EGFP show axonal blockages (arrows) similar to larvae expressing SGG^{WT} (B). (**K**) Quantification analysis shows that the extent of axonal blockages in SGG^{WT} ($P = 0.02784$), EGFP; SGG^{WT} ($P = 0.00538$) and SGG^{ACTIVE} ($P = 0.00721$) are significant. The extent of axonal blockages in PS+14.1 and SGG^{WT} or SGG^{ACTIVE} is significantly decreased compared with larvae expressing SGG^{WT} ($P = 0.04602$) or SGG^{ACTIVE} ($P = 0.01241$) alone. $N = 5$ larvae for each genotype from at least three independent genetic crosses. Data are presented as mean ± SEM (*$P < 0.05$, using Student's *t*-test). (**L**) Quantification analysis shows that the extent of axonal blockages in PSD447A is significant ($P = 4.48 \times 10^{-5}$). The extent of axonal blockages in PSD447A; SGG^{WT} or PSD447A; SGG^{ACTIVE} larvae compared with PSD447A ($P = 0.03108$), SGG^{WT} ($P = 0.00255$) or SGG^{ACTIVE} ($P = 0.00237$) was significant. $N = 5$ larvae for each genotype from at least three independent genetic crosses. Data are presented as mean ± SEM (*$P < 0.05$, **$P < 0.005$, ***$P < 0.0005$, using Student's *t*-test).

enhanced axonal blockages (51). Therefore, rescue of GSK3β-mediated axonal blocks could result by a stoichiometric requirement of functional PS.

PS undergoes endoproteolytic cleavage generating N- and C-terminal fragments (NTF and CTF) (19), which is essential for PS function (67). To further test that functional PS is required for GSK3β-mediated axonal transport, we used the FAD-linked *Drosophila* PS mutant PSD447A, which mimics the D385A amino acid substitution at the conserved aspartate residue within TM7 and encodes a non-functional form of PS that shows defective

endoproteolysis and γ-secretase activity (13). Intriguingly, larvae expressing PSD447A in all neurons showed CSP-positive axonal accumulations within their segmental nerves, in contrast to larvae expressing PS (Fig. 1G). Larvae expressing PSD447A in the context of excess SGG^{WT} also showed axonal blockages (Fig. 1H). Quantification of the average number of axonal blockages per larvae indicate that the extent of blockages in larvae expressing PSD447A with SGG^{WT} was significantly increased compared with larvae expressing PSD447A alone ($P < 0.05$) or SGG^{WT} ($P < 0.005$) alone (Fig. 1K). A similar increase in axonal blockages was also seen in larvae expressing PSD447A with SGG^{ACTIVE} ($P < 0.005$, Fig. 1I). These observations are consistent with our previous work that showed that larvae expressing SGG in the context of 50% reduction of PS enhanced GSK3β-mediated axonal blockages (51). Therefore, functional PS is required to rescue GSK3β-mediated axonal transport defects.

An intact PS loop is required to rescue GSK3β-mediated axonal transport defects

Studies have proposed that the hydrophilic loop region of PS binds GSK3β to mediate GSK3β dependent phosphorylation of β-catenin in the wnt-β-catenin signaling pathway (38–40). Similarly, perhaps the PS hydrophilic loop could also modulate GSK3β-mediated axonal transport defects. To test this possibility, we examined larvae expressing human PS loop or *Drosophila* PS loop in all neurons using the APPL-GAL4 driver. The UAS-human PS loop line expresses amino acids 263–407 of human PS which includes TM7 (68). The UAS-*Drosophila* PS (+14) loop line expresses the hydrophilic loop and TM7 following the loop (8). We found that similar to larvae expressing full-length PS, larvae expressing human PS loop (hPSloop) or *Drosophila* PS loop (dPSloop) alone showed smooth CSP stained segmental nerves which was comparable to WT larval nerves (Fig. 2D, Supplementary Material, Fig. S2). Strikingly, larvae expressing both SGG^{WT} and hPSloop or dPSloop showed smooth CSP staining with no axonal blockages, in contrast to larvae expressing SGG^{WT} alone (Fig. 2E, Supplementary Material, Fig. S2). Expression of hPSloop or dPSloop also rescued axonal blockages seen in larvae expressing SGG^{ACTIVE} (Fig. 2F, Supplementary Material, Fig. S2).

To further test that the loop region of PS is required for the modulation of GSK3β-mediated axonal transport defects, we examined larvae expressing the FAD mutant PSΔE9. In PSΔE9, residues 291–319, the part of the loop region encoded by exon 9 is deleted (30). This mutation fails to undergo endoproteolytic cleavage (19,31), but normal γ-secretase activity was seen (13). In contrast to larvae expressing dPSloop or hPSloop, larvae expressing PSΔE9 contained axonal blockages that stained with CSP (Fig. 2G). Larvae expressing both PSΔE9 and SGG^{WT} also contained axonal blockages (Fig. 2H). Similarly, larvae expressing both PSΔE9 and SGG^{ACTIVE} also showed axonal blockages (Fig. 2I). Quantification analysis revealed that the extent of blockages in larvae expressing both PSΔE9 and SGG^{ACTIVE} was significantly increased compared with larvae expressing SGG^{ACTIVE} ($P < 0.005$) alone or PSΔE9 ($P < 0.05$) alone. The increase in axonal blockages seen in larvae expressing both PSΔE9 and SGG^{WT} was significant compared with SGG^{WT} ($P < 0.05$) alone but not to PSΔE9 alone ($P > 0.05$). Although these observations indicate that the functional loop region of PS is required to rescue GSK3β-mediated axonal blockages, perhaps an intact PS loop may also be required to modulate GSK3β activity or motor binding to membranes. Indeed, exon 9 encompasses the GSK3β binding site on PS (41,42) and we previously showed that excess motor binding to membranes was correlated to axonal transport defects (51).

Functional PS and an intact PS loop are needed for proper kinesin and dynein binding to membranes

We previously showed that 50% reduction of PS decreased membrane binding of kinesin and dynein (51). The binding of active GSK3β to membranes was also decreased with 50% genetic reduction of PS (51). Similarly, 50% reduction of GSK3β/SGG also showed decreased membrane binding of active GSK3β and both kinesin and dynein (51). These studies propose that both PS and GSK3β are involved in mediating motor protein binding to membranes. In the wnt-β-catenin signaling pathway, binding of GSK3β to the hydrophilic loop of PS is proposed to mediate GSK3β dependent β-catenin phosphorylation (38–40). Therefore, the simplest prediction of how excess PS rescues GSK3β-mediated transport defects could be by binding GSK3β to the loop and titrating excess active GSK3β away from motors. This would prevent GSK3β from acting on motors, resulting in the decrease of motor binding to membranes. To test this prediction, we used biochemical analysis to fractionate membranes from adult fly brains expressing PS loop alone and adult fly brains expressing PSΔE9 alone. We found that the level of kinesin-1 was significantly increased in the membrane fraction from brains expressing PSΔE9 ($P < 0.005$, Student's *t*-test and Tukey's Honest Significant Difference (HSD) test and Bonferroni's test), while no changes were seen in brains expressing PS loop (Fig. 3B). The level of active GSK3β bound to membranes was also increased in brains expressing PSΔE9 but this increase was not significant. Therefore, an intact PS loop is required for the proper binding of kinesin and perhaps for the binding of active GSK3β to membranes.

To further test that functional PS also contributes to motor binding to membranes, we fractionated membranes from fly brains expressing PS+14 and brains expressing PSD447A, the non-functional form of PS that is defective in endoproteolysis and γ-secretase activity. We found that the level of both kinesin and dynein was increased in the membrane fraction from brains expressing PSD447A in contrast to brains expressing PS+14 alone (Fig. 4B, for kinesin-1 $P < 0.05$, Student's *t*-test, Tukey's HSD test and Bonferroni's test, for dynein $P < 0.005$, Student's *t*-test, Tukey's HSD test and Bonferroni's test). Interestingly, the level of active GSK3β was also increased in the membranes from brains expressing PSD447A in contrast to brains expressing PS+14 alone ($P < 0.005$, Student's *t*-test, Tukey's HSD test and Bonferroni's test). Therefore, a functional PS is essential for proper motor protein binding to membranes and for the membrane binding of active GSK3β.

Kinesin associates with active GSK3β and is phosphorylated *in vitro*

Previous studies in cells suggested that binding of kinesin-1 to membranes depends on the phosphorylation state of KLC, and that GSK3β-mediated phosphorylation of KLC releases kinesin from vesicles (53). Other work suggested that phosphorylation of kinesin heavy chain (KHC) can also induce membrane association (69). Therefore, one potential role for a functional PS and/or an intact loop region of PS is to bring active GSK3β to motors for their phosphorylation, similar to the mechanism proposed for β-catenin (38–40). One prediction of this proposal

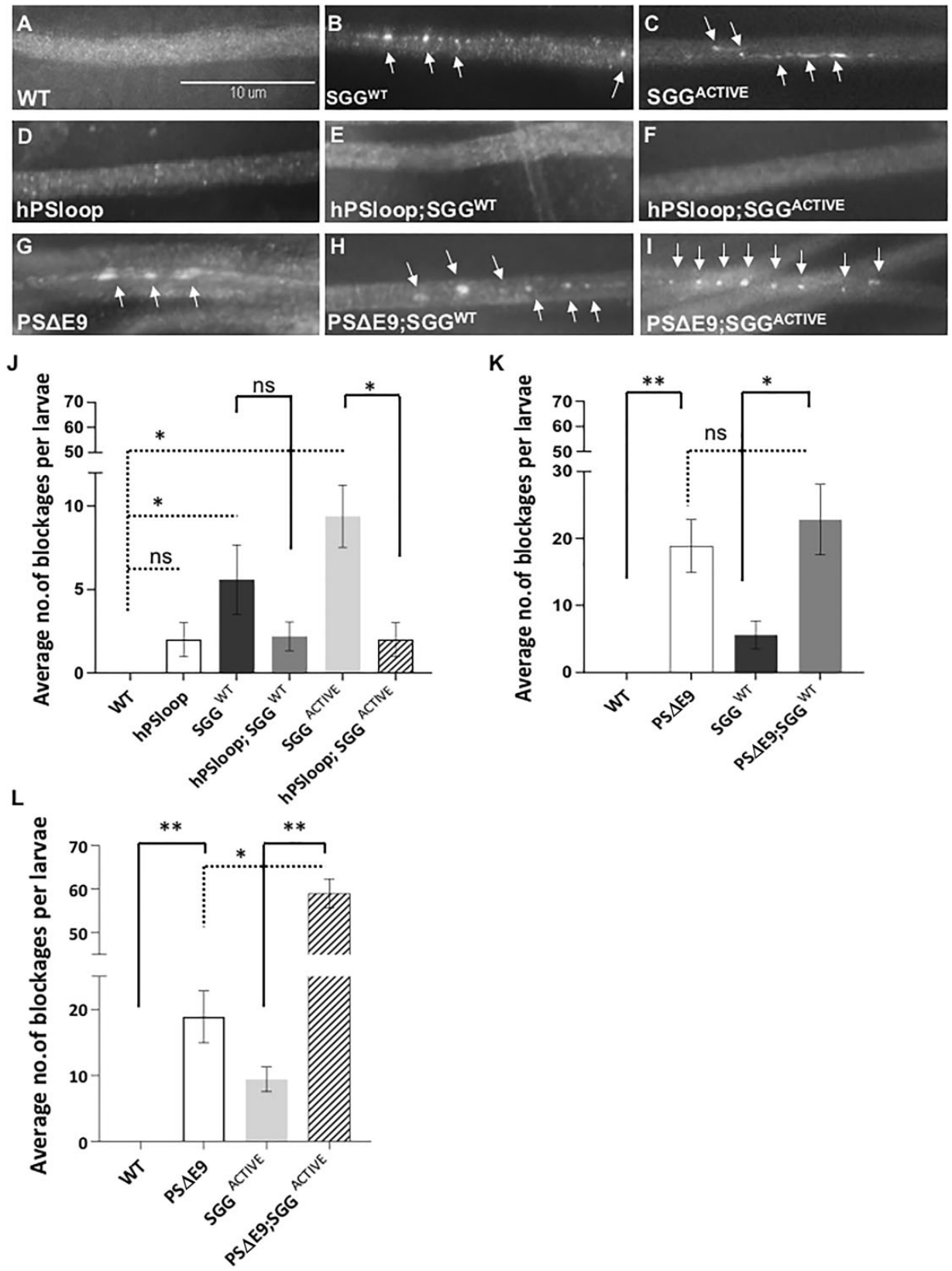

Figure 2. Expression of PS loop rescues GSK3β mediated transport defects. (**A–C**) A representative larval segmental nerve from WT larva and larva expressing SGG^{WT} or SGG^{ACTIVE} stained with the synaptic vesicle marker CSP. Note that the WT nerve shows smooth staining. In contrast, larval segmental nerves expressing SGG^{WT} or SGG^{ACTIVE} show axonal blockages (arrows). Scale Bar = 10 μm. (**D**) Larval segmental nerves from larvae expressing hPSloop show smooth staining. (**E** and **F**) Larval segmental nerves expressing hPSloop and SGG^{WT} or SGG^{ACTIVE} also show smooth staining. (**G**) Larval segmental nerves from larvae expressing PSΔE9 show axonal blockages (arrows). (**H** and **I**) Larval segmental nerves from larvae expressing PSΔE9 and SGG^{WT} or SGG^{ACTIVE} show axonal blockages (arrows). (**J**) Quantification analysis

is that active GSK3β and motors should associate. To test this possibility, using immunoprecipitation we isolated KHC from adult fly brains using an antibody against KHC. Western blot analysis showed that active GSK3β coimmunoprecipitated (co-IP) with KHC, indicating that KHC and active GSK3β can associate *in vitro* (Fig. 5A). Interestingly, our observations complement previous work that showed that GSK3β co-IPed with dynein intermediate chain (DIC) (70) and KLC (53), indicating that motors and GSK3β can exist as a complex.

A second prediction is that active GSK3β should phosphorylate motors. Indeed, early work showed that both KHC and KLC are endogenously phosphorylated (69,71), however, the identity of the kinase(s) responsible is not known. *Drosophila* KHC has two putative GSK3β phosphorylation sequences, one within the kinesin motor domain and the other within the stalk. To test whether *Drosophila* KHC is directly phosphorylated by GSK3β, we used an *in vitro* kinase assay. KHC was first isolated by immunoprecipitation from adult fly brain extracts and this fraction was incubated with recombinant glutathione S-transferase (GST) tagged active GSK3β in the presence of γ-^{32}P-ATP. Strikingly, the autorad showed a γ-^{32}P positive band at ~110 kDa corresponding to KHC (Fig. 5B). We also note that a γ-^{32}P positive band was seen at ~74 kDa which we predict is the autophosphorylation of GST-GSK-3β that was added to the reaction. Note that these bands disappear when the reaction was incubated with the GSK3β specific inhibitor CT99021, although the Coomassie gel still shows proteins. These observations are consistent with previous work using mouse brains that showed that dynein light chain, intermediate chain and light intermediate chains were all phosphorylated by GSK3β *in vitro* (70). Studies using rat brains indicated that KLC but not KHC was phosphorylated by GSK3β (53), however, here we demonstrate that KHC can also be phosphorylated by GSK3β.

GSK-3β influences the subcellular localization of PS within larval nerves

Previous studies showed that PS is an unprimed substrate of GSK3β (54) and that GSK3β activity modifies the localization and the function of PS (55). Typically, PS is localized to the endoplasmic reticulum and Golgi membranes (72). However, endogenous PS also localizes at the plasma membrane as an active molecule (73). In neurons, PS binds to β-catenin and N-(and E-) cadherin through the hydrophilic loop region at the synapse (11). Biochemical analysis showed that PS is also present in endocytic vesicles (32) and is part of APP-containing vesicles in mouse segmental neurons (48). Since we previously found that PS (49), like GSK3β (50) can control kinesin and dynein function during the axonal movement of APP *in vivo*, an alternative prediction of the hypothesis that PS and GSK3β are functionally coupled during axonal transport is that GSK3β influences the function of PS during axonal transport. To test this prediction, we evaluated the neuronal localization pattern of PS by generating larvae expressing GFP-tagged *Drosophila* PS in all neurons using the APPL-GAL4 driver, since a robust *Drosophila* PS antibody was unavailable. PS was present within the cell bodies in the larval brain and within larval nerves (Fig. 6A and B). Active GSK3β was also observed in larval brains (cell bodies, Supplementary Material, Fig. S4A), larval segmental nerves (Supplementary Material, Fig. S4B) as well as in the neuromuscular junctions (NMJs, Supplementary Material, Fig. S4C). Similar to larvae expressing PS+14 or PS−14, the GFP-PS expressing larvae also did not show axonal blockages (Fig. 6D, Supplementary Material, Fig. S1C).

To test how GSK3β influences the neuronal localization of PS, we generated larvae expressing both SGG^{WT} and GFP-PS. Axonal blockages mediated by excess SGG^{WT} were also rescued by expressing GFP-PS similar to Figure 1E, indicating that the N-terminal GFP-tagged PS was functional. Intriguingly, in contrast to larvae expressing GFP-PS alone, larvae expressing both SGG^{WT} and GFP-PS showed increased GFP-PS within cell bodies in the larval brain and very faint GFP-PS in larval nerves (Fig. 6E and F). Quantification analysis of four cell bodies each from eight larvae (total of 32) revealed a significant increase in the level of GFP-PS present in the cell bodies in larvae expressing SGG^{WT} and GFP-PS in contrast to larvae expressing GFP-PS alone ($P < 0.005$). In addition, a significant decrease was seen in the level of GFP-PS in these larval nerves compared with larvae expressing GFP-PS alone ($P < 0.005$). A similar phenotype was also seen in larvae expressing SGG^{ACTIVE} with GFP-PS (Fig. 6G and H). Since excess active GSK3β restricted GFP-PS to the cell bodies decreasing GFP-PS from the larval nerves, we predict that loss of GSK3β should disrupt this localization. To test this possibility, we generated larvae expressing SGG^{DN} and GFP-PS, since loss of function mutations of SGG result in embryonic lethality (74). Larvae expressing SGG^{DN} alone showed axonal blockages at levels greater than what was observed for larvae expressing SGG^{WT} or SGG^{ACTIVE} (Supplementary Material, Fig. S3B). In addition, western blot analysis of total proteins from brains expressing SGG^{DN} showed that the level of active GSK3β was significantly decreased (Supplementary Material, Fig. S3D and E, $P < 0.05$, Student's *t*-test, Tukey's HSD test and Bonferroni's test) compared with WT, indicating that SGG^{DN} likely functions as a hypomorph, consistent with what was previously shown (74). In contrast to larvae expressing GFP-PS and SGG^{WT}, larvae expressing both GFP-PS and SGG^{DN} showed increased GFP-PS within larval nerves (Fig. 6I and J). However, the level of GFP-PS in the cell bodies located in the larval brain was comparable to what was observed in larvae expressing GFP-PS alone (Fig. 6I and J). Taken together, our observations indicate that active GSK3β influences the subcellular localization of PS within larval nerves. Therefore, perhaps the GSK3β-mediated axonal blockages we observe in larval nerves (Figs 1–4) could be due to the restriction of PS to cell bodies. Although PS has two consensus phosphorylation sequences in its hydrophilic loop region (54,75), whether GSK3β-mediated phosphorylation is involved in the localization of PS is unknown.

shows that the extent of axonal blockages in SGG^{WT} ($P = 0.02784$), and SGG^{ACTIVE} ($P = 0.00721$) is significant, but the extent of axonal blockages in hPSloop is not ($P = 0.09718$). Note that while the extent of the decrease of axonal blockages in hPSloop; SGG^{WT} was not significant compared with SGG^{WT} ($P = 0.2738$), the extent of decrease of axonal blockages was significant in hPSloop; SGG^{ACTIVE} ($P = 0.0130$). $N = 5$ larvae for each genotype from at least three independent genetic crosses. Data are presented as mean ± SEM. (*$P < 0.05$, ns = non-significant, using two sided Student's *t*-test). (**K**) Quantification analysis shows that the extent of axonal blockages in larvae expressing PSΔE9 is significant ($P = 0.00134$) compared with WT. The extent of axonal blockages in larvae expressing PSΔE9 and SGG^{WT} is significant compared with SGG^{WT} alone ($P = 0.01847$) but is not compared with PSΔE9 alone ($P = 0.53979$). $N = 5$ larvae for each genotype from at least three independent genetic crosses. Data are presented as mean ± SEM (*$P < 0.05$, **$P < 0.005$, ns = non-significant, using two sided Student's *t*-test). (**L**) Quantification analysis shows that the extent of axonal blockages in larvae expressing PSΔE9 and SGG^{ACTIVE} is significantly increased compared with PSΔE9 alone ($P = 0.03475$) or SGG^{ACTIVE} alone ($P = 0.000576$). $N = 5$ larvae for each genotype from at least three independent genetic crosses. Data are presented as mean ± SEM (*$P < 0.05$, **$P < 0.005$, using Student's *t*-test).

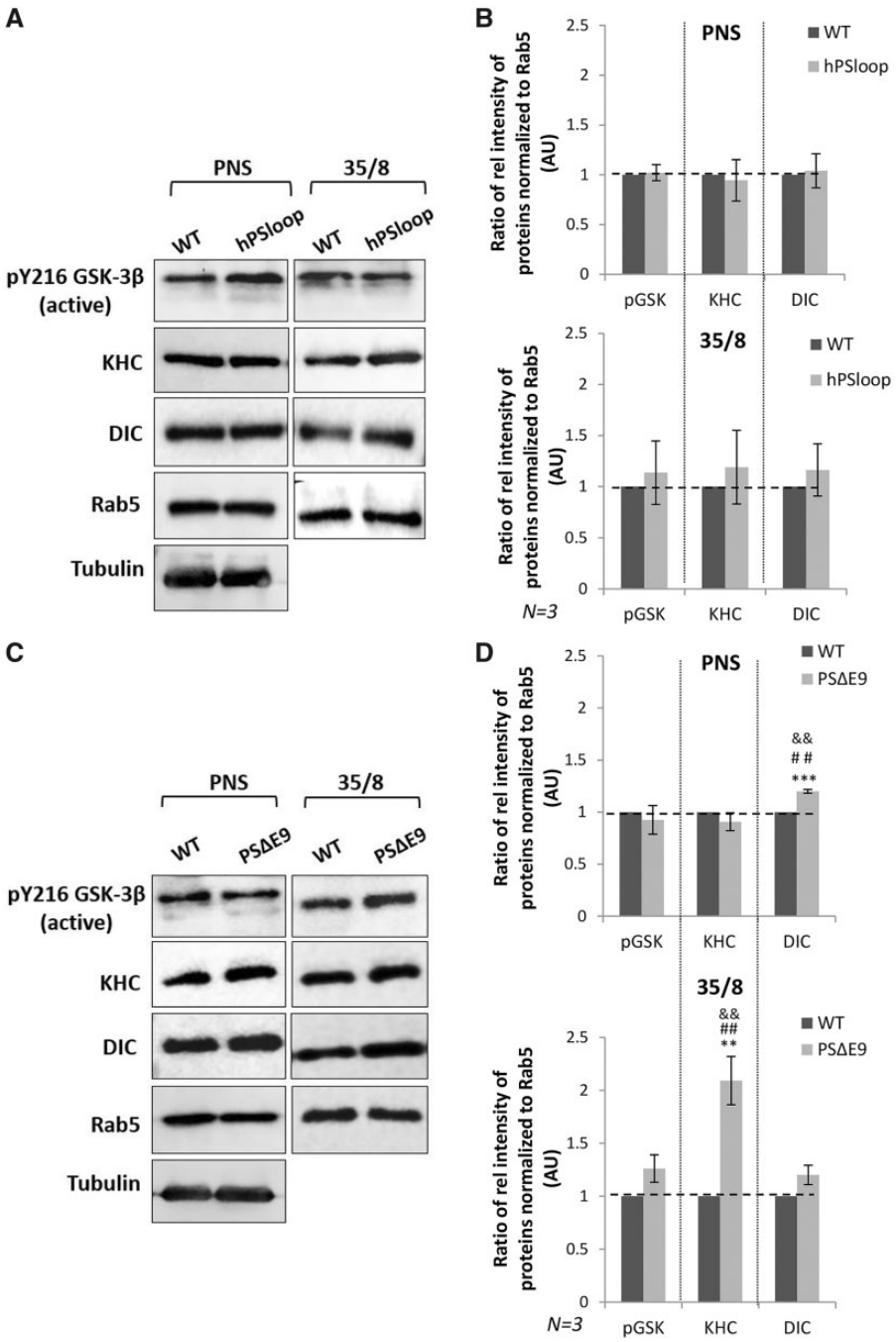

Figure 3. Deletion of PS loop increases motor binding to membranes. (**A**) Subcellular fractionation of adult fly brain membranes on sucrose step gradients from WT flies and flies expressing hPSloop show that the levels of active GSK3β, KHC and DIC bound to the membranes (35/8 fraction) are comparable. (**B**) Quantification analysis indicated that there were no significant changes in the levels of active GSK3β, KHC or DIC in the 35/8 fraction from hPSloop compared with WT (using Student's *t*-test). For quantification, the ratio of the intensity of KHC/DIC/active GSK3β for the PNS or the 35/8 fraction was determined against the intensity of Rab5 and normalized to WT from three independent experiments. Y axis depicts the intensity in arbitrary units (AU). Data are presented as mean ± SEM. (**C**) Subcellular fractionation of adult fly brain membranes from flies expressing PSΔE9 show that the level of active GSK3β and KHC bound to membranes were elevated compared with WT brains. (**D**) Quantification analysis indicates that the level of membrane bound KHC but not active GSK3β or DIC was significantly increased compared with WT. Statistical analysis using Student's *t*-test, Tukey's HSD test and Bonferroni's test indicate that only KHC levels were significant. For KHC, $^{**}P < 0.005$ ($P = 0.00425$) using Student's *t*-test, Tukey's HSD test (indicated by &&) and Bonferroni's test (indicated by ##). For active GSK3β, $P = 0.05374$ and for DIC, $P = 0.06909$ using Student's *t*-test, Tukey's HSD test and Bonferroni's test. Y axis depicts the intensity in AU. $N = 3$ independent experiments. Data are presented as mean ± SEM.

Discussion

We have identified a critical physiological role for the hydrophilic loop region of PS during GSK3β-mediated axonal transport using genetics, biochemistry and *in vivo* imaging in *Drosophila*. Our observations done in an intact organism allow us to propose a scaffolding mechanism for PS in regulating GSK3β-mediated functions on molecular motors during their motility *in vivo*. In contrast to the scaffolding role of PS proposed in the wnt-β-catenin

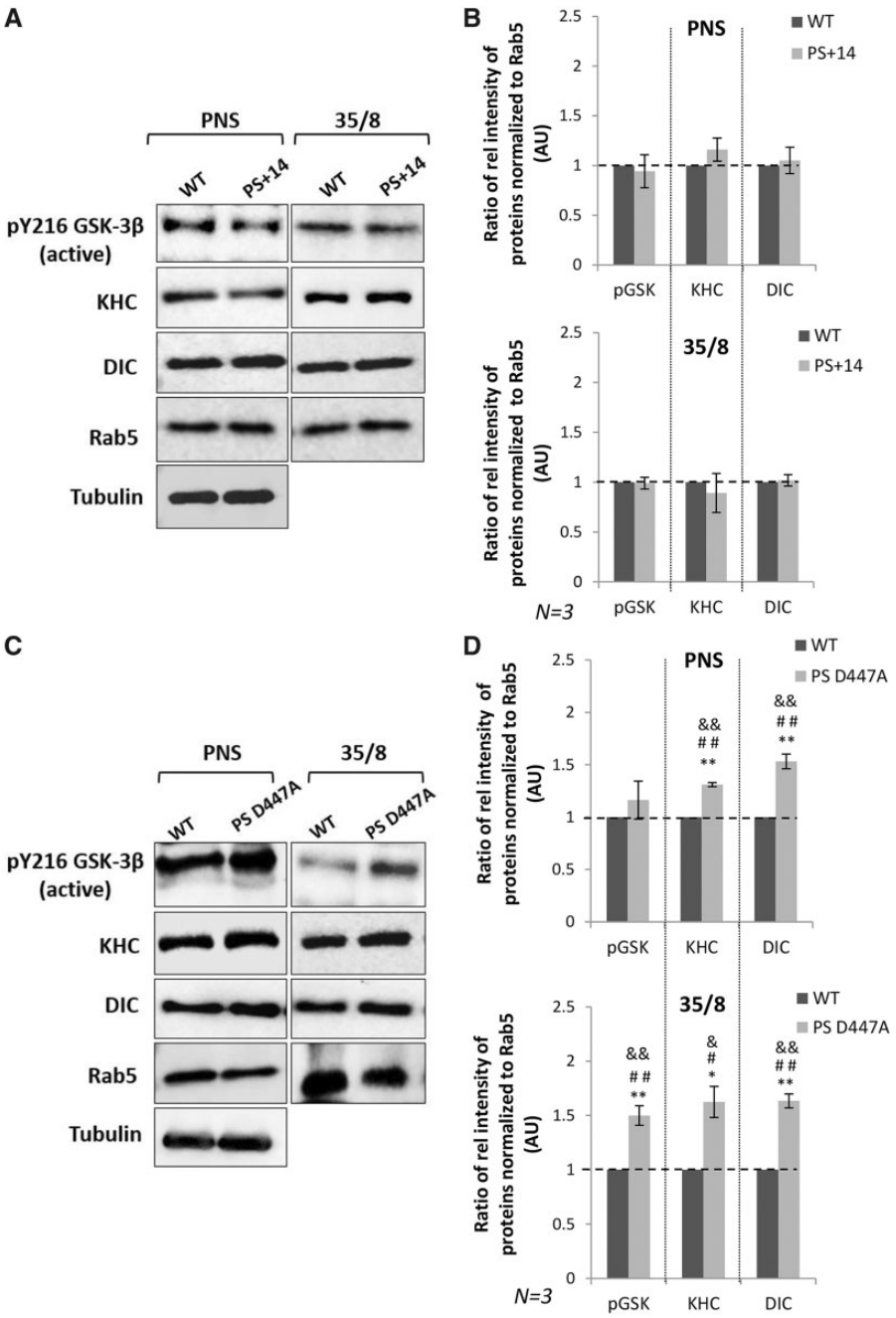

Figure 4. Non-functional PS increases active GSK3β and motor binding to membranes. (**A**) Subcellular fractionation of adult fly brain membranes on sucrose step gradients from flies expressing PS+14 show that the levels of active GSK3β, KHC and DIC bound to membranes are comparable to WT. (**B**) Quantification analysis indicated that there were no significant changes in the levels of active GSK3β, KHC and DIC in the 35/8 fraction compared with the WT (using Student's *t*-test). *Y* axis depicts the intensity in AU. $N = 3$ independent experiments. Data are presented as mean ± SEM. (**C**) Subcellular fractionation of adult brain membranes from flies expressing non-functional PS, PSD447A, show that the levels of active GSK3β, KHC and DIC bound to membrane was increased compared with WT. (**D**) For quantification, the ratio of the intensity of KHC/DIC/active GSK3β for the PNS or the 35/8 fraction was determined against the intensity of Rab5 and normalized to WT from three independent experiments. Statistical analysis using Student's *t*-test (**), Tukey's HSD test (&&) and Bonferroni's test (##) indicated that the changes were significant. For active GSK3β, $^{**}P < 0.005$ ($P = 0.00248$) using Student's *t*-test, Tukey's HSD test (indicated by &&) and Bonferroni's test (indicated by ##), for KHC $^{*}P < 0.05$ ($P = 0.0189$) using *t*-test, Tukey's HSD test (indicated by &) and Bonferroni's test (indicated by #) and for DIC $^{**}P < 0.05$ ($P = 0.00069$) using Student's *t*-test, Tukey's HSD test (indicated by &&) and Bonferroni's test (indicated by ##). *Y* axis depicts intensity in AU. $N = 3$ independent experiments. Data are presented as mean ± SEM.

signaling pathway, we report that the hydrophilic PS loop region likely sequesters GSK3β away from motors to rescue excess GSK3β-mediated axonal blockages. These findings have important implications for our understanding of the complex functions of PS and for the complicated regulatory mechanisms that must control motor protein activity during axonal transport *in vivo*.

A scaffolding role for PS during GSK3β-mediated axonal transport

In addition to the proteolysis function of PS, a scaffolding role for PS was demonstrated during β-catenin dependent signaling. Early work showed that β-catenin directly binds PS via the large hydrophilic loop domain (40,76,77). However, whether this

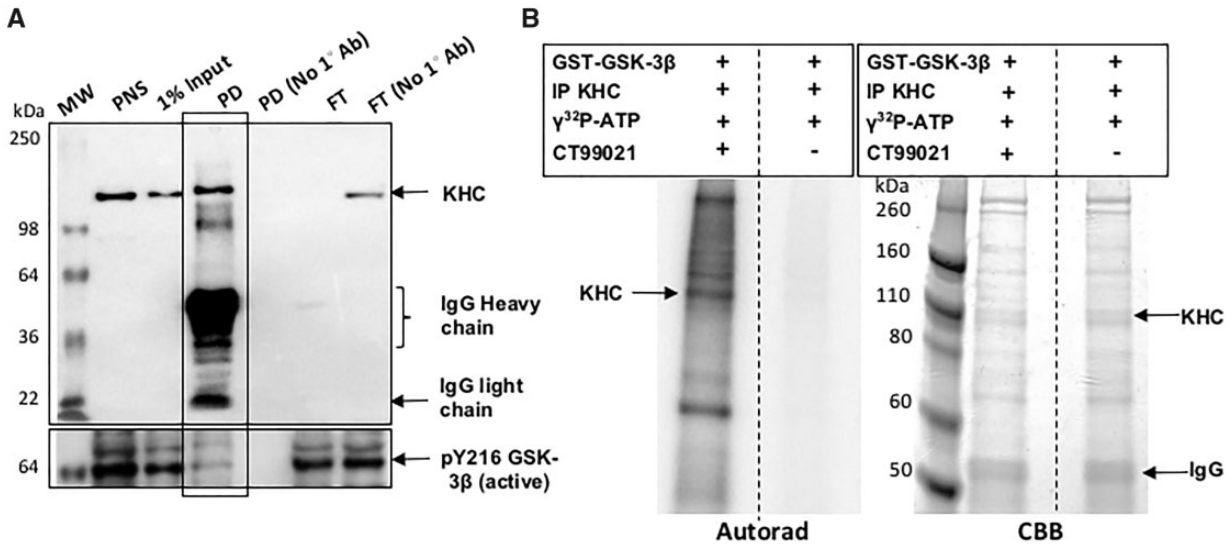

Figure 5. Kinesin and active GSK3β coimmunoprecipitate, and KHC is phosphorylated by GSK3β *in vitro*. (**A**) Kinesin was immunoprecipitated from fly heads using a KHC antibody. In the negative control KHC antibody was not used (No 1° Ab). Western blot analysis shows a band at ∼110 kDa in the KHC pull down (PD). Note that the flow through (FT) shows no KHC band indicating that all of KHC is likely immunoprecipitated, in contrast to the no antibody FT. Active GSK3β was detected in the KHC IP by the pY216 (active) GSK3β antibody but not all active GSK3β is present with KHC. MW, molecular weight marker. (**B**) KHC IP was used as the substrate in the *in vitro* kinase assay and was incubated with GST-GSK3β in the presence of 1mCi/100 γ^{32}P-ATP. As a control, this reaction was incubated with the GSK3β specific inhibitor CT99021. The autorad shows a strong band at ∼110 kDa indicating the phosphorylation of KHC. Note that a strong band is also observed at ∼74 kDa indicating that GSK3β is also autophosphorylated. Perhaps other proteins present in the KHC IP are also phosphorylated since all bands were absent in the reaction incubated with CT99021. However, note that the proteins are still present in both lanes in the Coomassie brilliant blue (CBB).

interaction stabilized β-catenin or enhanced the degradation of β-catenin was unclear. Although overexpression of WT PS in COS7 cells reduced cytoplasmic β-catenin, FAD PS mutants showed no effect (40). In contrast, overexpression of PS and β-catenin in HEK293 cells enhanced β-catenin stability, and this ability was decreased in FAD PS mutants (38). GSK3β bound to the N-terminal fragment of PS and β-catenin bound to the C-terminal fragment of PS facilitated the turnover of β-catenin (39). Further, these associations were decreased in FAD PSΔE9 indicating that the loop region plays an important role. Studies also proposed that PS was key in a stepwise phosphorylation mechanism of β-catenin, mediated first by PKA and then by GSK3β which ensures proper ubiquitination and degradation of β-catenin (37). Other work showed that phosphorylation of the serine residues in the hydrophilic loop region of PS by GSK3β induces a structural change in PS that reduces GSK3β interaction with β-catenin, decreasing β-catenin phosphorylation and ubiquination, stabilizing β-catenin (43). Although the scaffolding mechanism for PS has thus far been detailed only in the context of β-catenin signaling in *in vitro* studies, it is unclear whether such a mechanism exists *in vivo* and whether it is essential in the context of PS-mediated functions; to bring substrates for γ-secretase cleavage.

Our results here together with previous *in vivo* analysis in *Drosophila* indicate that the roles of PS (49) and GSK3β (50) are tightly coupled during axonal transport (51), enabling us to propose a scaffolding mechanism for PS in the regulation of GSK3β-mediated functions on motor proteins. Specifically, we propose a model in which the hydrophilic loop of PS is involved in facilitating GSK-3β-mediated functions on motor proteins. In this context at least two possibilities could exist. One possibility is that similar to the scaffolding role of PS in the wnt-β-catenin pathway, PS via its loop region brings GSK3β to motor proteins. An alternative possibility is that PS via its loop region sequesters GSK3β away from motors. Our observations favor a sequestering mechanism for the PS loop in titrating GSK3β away from motors (Supplementary Material, Fig. S5). Although we were unable to evaluate direct interactions between *Drosophila* PS and GSK3β due to the lack of robust antibodies, other work done in human, mice and monkey cells showed that GSK3β can bind to residues 250–298 of the PS loop (41) and that residues 263–298 of the PS loop is required for minimum binding of GSK3β (42). The PSΔE9 mutant lacking residues 219–391 showed decreased affinity for GSK3β (39). Additionally, KHC (Fig. 5A), KLC (53) or DIC (70) co-IP with GSK3β, indicating that motors and GSK3β can exist as a complex, similar to PS and GSK3β (39,41). Taken together, we propose that excess *Drosophila* PS loop or human PS loop rescues axonal blockages mediated by excess SGG^{WT} or SGG^{ACTIVE} (Fig. 2E and F, Supplementary Material, Fig. S1F and H) by binding excess GSK3β to the PS loop and titrating GSK3β away from motors (Supplementary Material, Fig. S5). Disruption of PS loop fails to titrate excess GSK3β away from motors enhancing GSK3β-mediated axonal blockages (Fig. 2H and I). However, in contrast to the wnt-β-catenin signaling pathway, our model predicts that PS-GSK3β and GSK3β-motor associations are independent, and that motors are unlikely to be in a PS-GSK3β complex (Supplementary Material, Fig. S5), as we previously observed that PS did not show obvious genetic interactions with kinesin-1 or dynein in the context of axonal blockages (49), unlike GSK3β and motors (50,51). Further, expression of full-length PS or PS loop had no effect on axonal transport (Figs 1D and 2D, Supplementary Material, Fig. S1C and E). Although further study is needed, whether excess PS-GSK3β are 'marked' for degradation however is unknown.

Our model is also consistent with the prediction that functional PS is also essential for the scaffolding mechanism of PS in GSK3β-mediated regulation of motor proteins during axonal transport. Expression of non-functional PS, PSD447A, that mimic a PS-null state with no endoproteolysis and γ-secretase

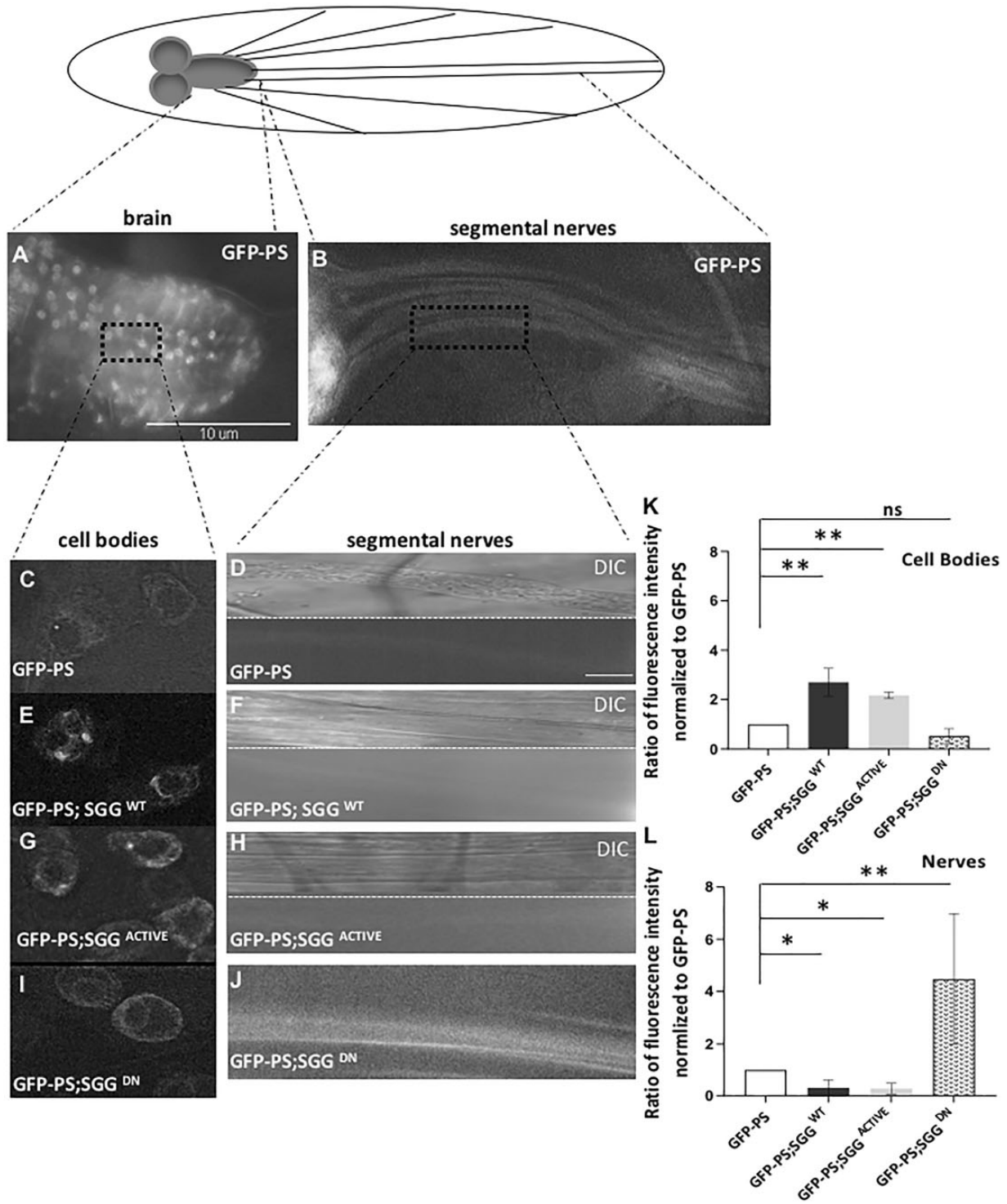

Figure 6. Expression of GSK3β influences the subcellular localization of PS. (**A–D**) A schematic diagram of the larval nervous system. GFP-PS is present in the larval brain and in the larval segmental nerves. Enlarged images at 100× show that GFP-PS is present in cell bodies and in the larval nerve. Differential interference contrast (DIC) microscopy images of the larval nerve are also shown. Scale Bar = 10 μm. (**E** and **F**) GFP-PS; SGG^{WT} larval brains show increased GFP-PS within the cell bodies and very faint GFP-PS in larval nerves. (**G** and **H**) Similarly larval brains expressing GFP-PS; SGG^{ACTIVE} show increased GFP-PS within the cell bodies and very faint GFP-PS in larval nerves. (**I** and **J**) In contrast, larvae expressing GFP-PS and SGG^{DN} show GFP-PS within cell bodies and within larval nerves. (**K** and **L**) Quantification analysis of four cell bodies each from eight larvae (total of 32 cell bodies) show significant increases in the level of GFP-PS in the cell bodies of larvae expressing GFP-PS; SGG^{WT} ($P = 0.00497$) and GFP-PS; SGG^{ACTIVE} ($P = 0.00263$) compared with larvae expressing GFP-PS alone. However, significant decreases in the level of GFP-PS is seen in the segmental nerves of larvae expressing GFP; SGG^{WT} ($P = 0.01545$) and GFP-PS: SGG^{ACTIVE} ($P = 0.005027$). $N = 8$ larval nerves. In contrast, GFP-PS; SGG^{DN} expressing larvae show significant increases in GFP-PS within larval segmental nerves ($P = 0.003217$) compared with GFP-PS larval nerves. However, the level of GFP-PS in cell bodies of GFP-PS; SGG^{DN} expressing larvae is comparable to GFP-PS alone ($P = 0.48172$). Data are presented as mean ± SEM. (*$P < 0.05$, **$P < 0.005$, Student's *t*-test). ns = non-significant.

activity also failed to rescue axonal blockages induced by excess SGG^{WT} or SGG^{ACTIVE} (Fig. 1H and I), but instead, enhanced blockages. These results are consistent with our previous work that showed that 50% reduction of PS (using the loss of function *Drosophila* PS mutant) in the context of excess SGG^{WT} or SGG^{ACTIVE} enhanced axonal blockages (51). However, unlike 50% reduction of PS, which showed decreased membrane binding of GSK3β (51), excess non-functional PS showed increased membrane binding of GSK3β, indicating that the non-functional PS, PSD447A does not fully mimic a PS-null state. One prediction is that PSD447A acts as a dominant negative in controlling GSK3β binding to membranes. Further, the PS and GSK3β association could be altered in PSD447A. Although the binding efficiency of GSK3β to PSD447A is unknown, GSK3β binding to the FAD mutant M146L was reduced (39). A second prediction is that structural modifications of the PS protein under physiological conditions could contribute to the complexity of PS functions on GSK3β during axonal transport *in vivo*. Indeed, endoproteolysis of PS is thought to cause conformational changes to the loop domains of PS (24). Phosphorylation of the PS loop region by GSK3β has also been proposed to cause structural changes that reduced interactions with β-catenin (43). Further, phosphorylation of PS at S367 in the loop causes a pathogenic 'closed' conformation (78), which was observed during both normal aging and in sporadic AD brains (79). Structural analysis and modeling studies showed that conformational modifications within the loop could directly control access to the channel-like interior and the catalytic site by a 'gate-plug' mechanism (25,26). Therefore, an aberrant conformational structure of the FAD PSD447A mutant which lacks both endoproteolysis and γ-secretase activities could be responsible for the dominant negative behaviors we observe.

GSK3β-mediated phosphorylation of motor proteins and PS during axonal transport

Our scaffolding mechanism for GSK3β-mediated regulation of axonal transport predicts that GSK3β and motors must associate (Supplementary Material, Fig. S5) perhaps for phosphorylation. Indeed, we found that KHC and active GSK3β are directly associated in co-IP analysis using fly brains (Fig. 5A). Work in mice and rats showed that GSK3β and DIC (70) or KLC (53) associate in co-IP analysis. However, whether active GSK3β also associates with DIC and KLC is unclear. Together, these studies indicate that motors and GSK3β can exist as a complex. A second prediction of our scaffolding model is that GSK3β should directly phosphorylate motor proteins. Indeed, we found that KHC isolated from fly brains was phosphorylated by active GSK3β in an *in vitro* kinase assay (Fig. 5B). Phosphorylation of KHC and autophosphorylation of GSK3β was inhibited by the GSK3β specific inhibitor CT99021 (Fig. 5C). Further, dynein light chain, intermediate chain and light intermediate chains were all shown to be phosphorylated by GSK3β *in vitro* in mouse brains (70). In rat brain extracts, KLC, but not KHC was shown to be phosphorylated by GSK3β (53). Perhaps the discrepancy in GSK3β-mediated phosphorylation of KHC in flies versus mice could be due to the fact that flies only have one KHC gene which contains putative GSK3β phosphorylation consensus sequences (51), while mammals have three KHC genes (KIF5A, B, C) with diverse expression patterns in different tissues/cells (80–83). KIF5A and KIF5C are expressed in neuronal tissues while KIF5B is ubiquitous (83). Intriguingly, sequence analysis shows that KIF5A and KIF5B contain putative GSK3β phosphorylation consensus sequences, while KIF5C does not. Additionally, since mammalian KHC and KLC genes also have sites for 5' adenosine monophosphate-activated protein kinase (AMPK) phosphorylation (84) and sites for other kinases (85,86), perhaps specific kinases function to regulate motor subunits or to dictate functional specificity during axonal transport.

Phosphorylation of motors by GSK3β could mediate motor protein attachment to membranes, motor detachment from membranes or motor activity during axonal transport. It is thought that kinesin-1 motors adopt a folded compact conformation which is inactive or an extended, linear conformation which is active (87). *In vitro* experiments using GST-tagged kinesin showed that kinesin-1 motors on purified membranes were inactive, while attached to cargo (71,88). However, in other work, phosphorylation was shown to play a role in relieving the autoinhibition of two mitotic kinases (89). Although the mechanisms of kinesin-1 phosphorylation in the context of axonal transport are still unknown, several observations from cells, mice and flies hint at an important role for GSK3β-mediated phosphorylation. Increased GSK3β activity increased the levels of KLC phosphorylation leading to a reduction in membrane bound kinesin-1, disrupting anterograde transport in squid axoplasm (53,90). However, in other studies KHC phosphorylation induced membrane associations in mammalian cells (69). In another study kinesin motor activity, not membrane binding was proposed to be regulated by phosphorylation (71). Previously, we showed that genetic reduction of endogenous GSK3β in flies decreased motor binding to membranes, while excess of active GSK3β increased motor binding to membranes (51). Our observations here indicate that motor binding to membranes is coupled to active GSK3β (Figs 3 and 4), that active GSK3β restricts the localization of PS to cell bodies, preventing its function in the axon (Fig. 6), and that excess motors on membranes can cause axonal blockages. Therefore, while it is clear that GSK3β-mediated phosphorylation likely plays key roles in motor regulation, further investigations are needed to unravel the mechanistic details under physiological conditions.

In the scaffolding mechanism for β-catenin signaling, phosphorylation of PS at serine residues in the loop domain was proposed to negatively regulate the formation of the ternary complex between β-catenin, PS and GSK3β leading to decreased degradation and stabilization of β-catenin (43). Similarly, phosphorylation of PS at its loop domain could act as the switch that controls the GSK3β-mediated activities on motors. In our scaffolding model, a conformation change mediated by phosphorylation of PS loop could perhaps initiate GSK3β-PS interactions preventing associations between GSK3β and motors, thus regulating GSK3β-mediated effects on motors. Alternatively, GSK3β may dictate the subcellular localization of PS, restricting the functions of PS during axonal transport to a specific cellular compartment. Typically, PS has been shown to be localized mainly to the endoplasmic reticulum and Golgi membranes (72). However, endogenous PS was also found at the plasma membrane as an active molecule (73). In neurons, at synapses PS1 binds β-catenin and N-(and E-) cadherin through its hydrophilic loop (11). Uemura *et al.* (55), showed that GSK3β-mediated phosphorylation of PS1 reduced its binding to N-cadherin and downregulated the cell-surface expression of PS in CHO cells. PS was also proposed to be present within APP vesicles in axons (48). Our observations showed that excess active GSK3β increased PS localization to the cell bodies decreasing its entry into axons, while reduction of GSK3β increased PS localization to axons (Fig. 6I and J). Therefore, complex formation between PS and GSK3β could control the subcellular localization of PS

thereby negatively mediating the subcellular compartment where GSK3β-mediated functions on motor proteins occur. Perhaps this is the reason for why reduction of PS and GSK3β only influenced the axonal motility of APP vesicles and not SYNT vesicles (49,50). Intriguingly, our previous observations showed that excess of PS or PS loop rescued APP-mediated axonal transport defects (91), indicating that APP is likely a key player in PS-GSK3β-mediated effects on axonal transport. Further studies are needed to test predictions of this proposal.

In summary, our observations suggest a scaffolding mechanism for PS in which the hydrophilic loop region sequesters GSK3β away from motors likely to control motor activities during axonal transport *in vivo* (Supplementary Material, Fig. S5). Although functional PS is also required, PS appears to act as the switch that negatively influences associations between GSK3β and motors during axonal transport. Further investigations in an *in vivo* system are needed to identify the mechanistic details of how GSK3β influences motor binding/release from membranes and/or motor activity. Thus our work highlights a key role for PS that is likely independent of its γ-secretase activity.

Materials and Methods

Drosophila genetics

Seven transgenic *Drosophila* PS lines UAS-PS+14, UAS-PS−14, UAS-hPSloopA8, UAS-dPSloop, UAS-PSΔE9, UAS-PSD447A and UAS-GFP-PS and three transgenic GSK3β lines, UAS-SGGB (SGG^{WT}), UAS-SGGS9A (SGG^{ACTIVE}) and UAS-SGGA81T (SGG^{DN}) were used. UAS-PS+14, UAS-PS−14 and UAS-dPSloop were obtained from Dr Mark E. Fortini and UAS-hPSloopA8 flies were obtained from Dr Norbert Perrimon. UAS-PSΔE9 and UAS-PSD447A and UAS-EGFP flies were obtained from Bloomington Stock Center. The UAS-GFP-PS line was generated by isolating *Drosophila* PS from cDNA clone LD23505 and cloning a 2072 bp insert into pUAST-NT-GFP (Richard Brusch). The pUAST-GFP-PS construct was injected into white eye *Drosophila* embryos and transformants were selected using eye color (GenetiVision). The pan neuronal driver APPL-GAL4 was used for neuronal expression of transgenic lines. For genetic interaction analysis, UAS-PS males were first crossed to APPL-GAL4; T(2:3), CyO, TM6B, Tb/Pin88K virgin females to obtain APPL-GAL4/y; UAS-PS/T(2:3), CyO, TM6B and Tb males. The chromosome carrying T(2:3), CyO, TM6B and Tb is referred to as B3 and carries the dominant markers, Hu, Tb and CyO. The larval Tb (tubby) marker is used to select larvae. The APPL-GAL4/y; UAS-PS/B3 males were crossed to virgin females that were UAS-SGGB(SGG^{WT}), UAS-SGGS9A (SGG^{ACTIVE}) or UAS-SGGA81T (SGG^{DN}), and non-tubby female larvae were dissected for immunohistochemistry. Sibling tubby larvae were evaluated as controls. Reciprocal crossings were also done to confirm observations. As a control, males that were APPL-GAL4/y; UAS-EGFP/B3 were also crossed to UAS-SGGB (SGG^{WT}).

Larval preparations, immunohistochemistry and quantifications

Third instar larvae were dissected, fixed and segmental nerves were immunostained as previously described (92). Briefly, larvae were dissected in dissection buffer (2× stock containing 128 mM NaCl, 4 mM $MgCl_2$, 2 mM KCl, 5 mM HEPES and 36 mM sucrose, pH 7.2). Dissected larvae were fixed in 8% paraformaldehyde, washed with PBT (phosphate buffered saline supplemented with 0.1% Tween-20) and incubated overnight with antibodies against CSP (1:10, Developmental Studies Hybridoma Bank) or pGSK3β (1:1000, Abcam). Larvae were incubated in secondary antibodies (Alexa anti-mouse 568, 1:100, Invitrogen) and mounted using Vectashield mounting medium (Vector Labs). Images of segmental nerves were collected using a Nikon Eclipse TE 2000U microscope using the 40× objective, and NMJs and cell bodies were imaged using the 100× objective (Nikon, Melville, NY, USA) microscope. Quantitative analysis on the extent of blockages was carried out by collecting six confocal optical images from larval neurons from the region directly below or posterior to the larval brain, where several segmental nerves are visible or come into focus through the optical series. For each genotype, five to seven animals were imaged, and nerves were analyzed over a length of 50 μm, using the threshold, density slice and particle analysis functions in NIH ImageJ software as previously described (52).

Membrane flotation and western blot analysis

Five milliliters of larval brains from each genotype (UAS-PS+14, UAS-PS−14, UAS-hPSloopA8, UAS-dPSloop, UAS-PSΔE9 and UAS-PSD447A) were collected and homogenized in acetate buffer (10 mM HEPES, pH 7.4, 100 mM K acetate, 150 mM sucrose, 5 mM EGTA, 3 mM Mg acetate, 1 mM DTT) with proteinase inhibitor (Roche) and phosphatase inhibitor (Invitrogen) (51,61). The homogenate was centrifuged at 1000*g* for 10 min and the debris were discarded. The resulting PNS was brought to 40% sucrose. This mixture was overlaid with cushions of 35 and 8% sucrose and the gradient was centrifuged at 50 000*g* for 1.5 h in a TLS55 rotor (Beckman Coulter, Fullerton, CA, USA). Vesicles, membranous organelles and membrane-associated proteins were found at the 35/8 interface, while heavier membranes and mitochondria were found in the pellet. Equal amounts of protein from the PNS, 35/8 interface, soluble and pellet fractions were analyzed by western blotting. Antibodies pY216 GSK3β monoclonal antibody (Abcam at 1:1000), GSK3β total polyclonal antibody (Cell Signaling at 1:1000), anti-KHC polyclonal antibody (Cytoskeleton at 1:1000), anti-DIC monoclonal antibody (Abcam at 1:1000), anti-Rab5 polyclonal antibody (Abcam 1:1000) and anti-tubulin monoclonal antibody (Invitrogen at 1:1000 dilution) were used. Immunoreactions were detected using the SuperSignal West Femto Maximum sensitivity substrate (Invitrogen) and imaged using QuantityOne (Bio-Rad). Quantification analysis was performed using Imagelab software. Relative intensities was calculated by dividing the intensity value for each sample by the intensity value of Rab5 and then normalized to WT, so that WT was 1. Statistical significance was calculated using two-sample two-sided Student's *t*-test, Tukey's HSD test and Bonferroni's test, specially designed to compare each treatment with a control. Differences were considered significant at a significance level of 0.05, which means a 95% statistically significant correlation from three separate membranes from three independent experiments.

Fly head extract preparation and KHC Immunoprecipitation

For preparation of *Drosophila* head extracts, 8 ml of fly heads from WT flies were homogenized in acetate buffer as previously described (51,61). The lysate was centrifuged at 1000*g* for 10 min at 4°C. Concentrations of the extracts were determined using bicinchoninic acid (BCA) protein assay (Pierce). For IP, 2 mg of the fly head lysate was incubated overnight with 4 μg KHC

antibody (Cytoskeleton) at 4°C. Protein A/G Magnetic Beads (Pierce) washed in wash buffer (Tris-buffered saline containing 0.05% Tween-20) was added to the mixture and incubated at room temperature for 1 h. Magnetic beads were then eluted in 100 μl low pH elution buffer (Pierce). The low pH was neutralized by adding 15 μl Tris pH 8.8. The concentration of the KHC pull down was determined by BCA assay. Western blot analysis was used to evaluate the extent and purity of the KHC immunoprecipitation as seen in Figure 5A.

In vitro GSK3β phosphorylation assay

Recombinant GST-GSK3β (SignalChem) was used for the *in vitro* kinase assay. Potential substrates (KHC IP) were incubated with 50 ng GSK3β and 1mCi/100 γ^{32}P-ATP for 30 min at 37°C. The reaction was terminated using 4X sample buffer. Control reactions containing 3 μM of GSK3β inhibitor CT99021 (Selleck) were done to evaluate the specificity of the GSK3β phosphorylation assay. Proteins were separated by SDS-PAGE, the gel was dried and sealed in saran wrap and exposed to X-ray film overnight. After exposure, gels were stained with Coomassie brilliant blue to visualize proteins.

Statistical analysis

For immunofluorescence analysis of axonal blockages, statistical analysis was performed in Excel (Microsoft Corp.), using the two-sample two-sided Student's *t*-test. Differences were considered significant at a significance level of 0.05, which means a 95% statistically significant correlation for 5–10 individual larvae from several independent crosses. For western blots, quantification analysis was performed using Image Lab software. Data obtained from Image Lab was analyzed in Excel (Microsoft Corp.) using two-sided Student's *t*-test. Additionally, Bonferroni's test and Tukey's HSD test was performed in Minitab 18. Both of the methods are pair-wise multiple comparison procedures specifically designed to compare each treatment with a control (93,94). Differences were considered significant at a significance level of 0.05, which means a 95% statistically significant correlation from three separate membranes from three independent experiments.

Supplementary Material

Supplementary Material is available at *HMG* online.

Acknowledgements

The authors thanks the members of the Gunawardena Lab for their constructive discussions and insight. The authors also thank Drs Mark E Fortini and Norbert Perrimon for providing the transgenic PS fly lines. S.G. thanks Priyantha Karunaratne for constant support. This work is dedicated to the memory of Richard Brusch.

Conflict of Interest statement. None declared.

Funding

This work was supported in part by funds from NIH/NINDS (R03-NS084386 and R03-NS092024) and by a grant from the Office of the Vice President for Research and Economic Development (OVPRED) from SUNY at Buffalo to S.G. R.B. was supported in part by the Mark Diamond Research Fund from SUNY at Buffalo, Z.R. and C.N. were supported by fellowships from the Center for Undergraduate Research and Creative Activities (CURCA) from SUNY at Buffalo. C.N. was also supported by a fellowship by a Collegiate Science and Technology Entry Program (CSTEP) research fellowship from SUNY at Buffalo.

References

1. Laudon, H., Hansson, E.M., Melen, K., Bergman, A., Farmery, M.R., Winblad, B., Lendahl, U., von Heijne, G. and Naslund, J. (2005) A nine-transmembrane domain topology for presenilin 1. *J. Biol. Chem.*, **280**, 35352–35360.
2. Sherrington, R., Rogaev, E.I., Liang, Y., Rogaeva, E.A., Levesque, G., Ikeda, M., Chi, H., Lin, C., Li, G. and Holman, K. (1995) Cloning of a gene bearing missense mutations in early-onset familial Alzheimer's disease. *Nature*, **375**, 754–760.
3. Doan, A., Thinakaran, G., Borchelt, D.R., Slunt, H.H., Ratovitsky, T., Podlisny, M., Selkoe, D.J., Seeger, M., Gandy, S.E. and Price, D.L. (1996) Protein topology of presenilin 1. *Neuron*, **17**, 1023–1030.
4. Shen, J., Bronson, R.T., Chen, D.F., Xia, W., Selkoe, D.J. and Tonegawa, S. (1997) Skeletal and CNS defects in presenilin-1-deficient mice. *Cell*, **89**, 629–639.
5. Wong, P.C., Zheng, H., Chen, H., Becher, M.W., Sirinathsinghji, D.J., Trumbauer, M.E., Chen, H.Y., Price, D.L., Van der Ploeg, L.H. and Sisodia, S.S. (1997) Presenilin 1 is required for Notch1 and DII1 expression in the paraxial mesoderm. *Nature*, **387**, 288–292.
6. De Strooper, B., Saftig, P., Craessaerts, K., Vanderstichele, H., Guhde, G., Annaert, W., Von Figura, K. and Van Leuven, F. (1998) Deficiency of presenilin-1 inhibits the normal cleavage of amyloid precursor protein. *Nature*, **391**, 387–390.
7. Struhl, G. and Greenwald, I. (1999) Presenilin is required for activity and nuclear access of Notch in Drosophila. *Nature*, **398**, 522–525.
8. Ye, Y., Lukinova, N. and Fortini, M.E. (1999) Neurogenic phenotypes and altered Notch processing in Drosophila Presenilin mutants. *Nature*, **398**, 525–529.
9. Berridge, M.J. (2011) Calcium signalling and Alzheimer's disease. *Neurochem. Res.*, **36**, 1149–1156.
10. Rajendran, L. and Annaert, W. (2012) Membrane trafficking pathways in Alzheimer's disease. *Traffic*, **13**, 759–770.
11. Georgakopoulos, A., Marambaud, P., Efthimiopoulos, S., Shioi, J., Cui, W., Li, H.C., Schutte, M., Gordon, R., Holstein, G.R. and Martinelli, G. (1999) Presenilin-1 forms complexes with the cadherin/catenin cell-cell adhesion system and is recruited to intercellular and synaptic contacts. *Mol. Cell*, **4**, 893–902.
12. Donoviel, D.B., Hadjantonakis, A.K., Ikeda, M., Zheng, H., Hyslop, P.S. and Bernstein, A. (1999) Mice lacking both presenilin genes exhibit early embryonic patterning defects. *Genes Dev.*, **13**, 2801–2810.
13. Wolfe, M.S., Xia, W., Ostaszewski, B.L., Diehl, T.S., Kimberly, W.T. and Selkoe, D.J. (1999) Two transmembrane aspartates in presenilin-1 required for presenilin endoproteolysis and gamma-secretase activity. *Nature*, **398**, 513–517.
14. Steiner, H., Duff, K., Capell, A., Romig, H., Grim, M.G., Lincoln, S., Hardy, J., Yu, X., Picciano, M., Fechteler, K. *et al.* (1999) A loss of function mutation of presenilin-2 interferes with amyloid beta-peptide production and notch signaling. *J. Biol. Chem.*, **274**, 28669–28673.

15. Rademakers, R., Cruts, M. and Van Broeckhoven, C. (2003) Genetics of early-onset Alzheimer dementia. *ScientificWorldJournal*, **3**, 497–519.
16. Lukinova, N.I., Roussakova, V.V. and Fortini, M.E. (1999) Genetic characterization of cytological region 77A-D harboring the presenilin gene of Drosophila melanogaster. *Genetics*, **153**, 1789–1797.
17. Marfany, G., Del-Favero, J., Valero, R., De Jonghe, C., Woodrow, S., Hendriks, L., Van Broeckhoven, C. and Gonzalez-Duarte, R. (1998) Identification of a Drosophila presenilin homologue: evidence of alternatively spliced forms. *J. Neurogenet.*, **12**, 41–54.
18. Ye, Y. and Fortini, M.E. (1998) Characterization of Drosophila Presenilin and its colocalization with Notch during development. *Mech. Dev.*, **79**, 199–211.
19. Thinakaran, G., Borchelt, D.R., Lee, M.K., Slunt, H.H., Spitzer, L., Kim, G., Ratovitsky, T., Davenport, F., Nordstedt, C., Seeger, M. *et al.* (1996) Endoproteolysis of presenilin 1 and accumulation of processed derivatives in vivo. *Neuron*, **17**, 181–190.
20. Podlisny, M.B., Citron, M., Amarante, P., Sherrington, R., Xia, W., Zhang, J., Diehl, T., Levesque, G., Fraser, P., Haass, C. *et al.* (1997) Presenilin proteins undergo heterogeneous endoproteolysis between Thr291 and Ala299 and occur as stable N- and C-terminal fragments in normal and Alzheimer brain tissue. *Neurobiol. Dis.*, **3**, 325–337.
21. Campbell, W.A., Reed, M.L., Strahle, J., Wolfe, M.S. and Xia, W. (2003) Presenilin endoproteolysis mediated by an aspartyl protease activity pharmacologically distinct from gamma-secretase. *J. Neurochem.*, **85**, 1563–1574.
22. Borchelt, D.R., Thinakaran, G., Eckman, C.B., Lee, M.K., Davenport, F., Ratovitsky, T., Prada, C.M., Kim, G., Seekins, S., Yager, D. *et al.* (1996) Familial Alzheimer's disease-linked presenilin 1 variants elevate Abeta1-42/1-40 ratio in vitro and in vivo. *Neuron*, **17**, 1005–1013.
23. Steiner, H., Romig, H., Grim, M.G., Philipp, U., Pesold, B., Citron, M., Baumeister, R. and Haass, C. (1999) The biological and pathological function of the presenilin-1 Deltaexon 9 mutation is independent of its defect to undergo proteolytic processing. *J. Biol. Chem.*, **274**, 7615–7618.
24. Knappenberger, K.S., Tian, G., Ye, X., Sobotka-Briner, C., Ghanekar, S.V., Greenberg, B.D. and Scott, C.W. (2004) Mechanism of gamma-secretase cleavage activation: is gamma-secretase regulated through autoinhibition involving the presenilin-1 exon 9 loop? *Biochemistry*, **43**, 6208–6218.
25. Li, Y., Bohm, C., Dodd, R., Chen, F., Qamar, S., Schmitt-Ulms, G., Fraser, P.E. and St George-Hyslop, P.H. (2014) Structural biology of presenilin 1 complexes. *Mol. Neurodegener.*, **9**, 59.
26. Somavarapu, A.K. and Kepp, K.P. (2016) The dynamic mechanism of presenilin-1 function: sensitive gate dynamics and loop unplugging control protein access. *Neurobiol. Dis.*, **89**, 147–156.
27. Woodruff, G., Young, J.E., Martinez, F.J., Buen, F., Gore, A., Kinaga, J., Li, Z., Yuan, S.H., Zhang, K. and Goldstein, L.S. (2013) The presenilin-1 DeltaE9 mutation results in reduced gamma-secretase activity, but not total loss of PS1 function, in isogenic human stem cells. *Cell Rep.*, **5**, 974–985.
28. Saura, C.A., Choi, S.-Y., Beglopoulos, V., Malkani, S., Zhang, D., Rao, B.S.S., Chattarji, S., Kelleher, R.J., Kandel, E.R., Duff, K. *et al.* (2004) Loss of presenilin function causes impairments of memory and synaptic plasticity followed by age-dependent neurodegeneration. *Neuron*, **42**, 23–36.
29. Kelleher, R.J., III and Shen, J. (2017) Presenilin-1 mutations and Alzheimer's disease. *Proc. Natl. Acad. Sci. U. S. A.*, **114**, 629–631.
30. Perez-Tur, J., Froelich, S., Prihar, G., Crook, R., Baker, M., Duff, K., Wragg, M., Busfield, F., Lendon, C. and Clark, R.F. (1995) A mutation in Alzheimer's disease destroying a splice acceptor site in the presenilin-1 gene. *Neuroreport*, **7**, 297–301.
31. Lee, M.K., Borchelt, D.R., Kim, G., Thinakaran, G., Slunt, H.H., Ratovitski, T., Martin, L.J., Kittur, A., Gandy, S., Levey, A.I. *et al.* (1997) Hyperaccumulation of FAD-linked presenilin 1 variants in vivo. *Nat. Med.*, **3**, 756–760.
32. Kim, S.H., Leem, J.Y., Lah, J.J., Slunt, H.H., Levey, A.I., Thinakaran, G. and Sisodia, S.S. (2001) Multiple effects of aspartate mutant presenilin 1 on the processing and trafficking of amyloid precursor protein. *J. Biol. Chem.*, **276**, 43343–43350.
33. Kimberly, W.T., Xia, W., Rahmati, T., Wolfe, M.S. and Selkoe, D.J. (2000) The transmembrane aspartates in presenilin 1 and 2 are obligatory for gamma-secretase activity and amyloid beta-protein generation. *J. Biol. Chem.*, **275**, 3173–3178.
34. Ray, W.J., Yao, M., Mumm, J., Schroeter, E.H., Saftig, P., Wolfe, M., Selkoe, D.J., Kopan, R. and Goate, A.M. (1999) Cell surface presenilin-1 participates in the gamma-secretase-like proteolysis of Notch. *J. Biol. Chem.*, **274**, 36801–36807.
35. Berezovska, O., Jack, C., McLean, P., Aster, J.C., Hicks, C., Xia, W., Wolfe, M.S., Kimberly, W.T., Weinmaster, G., Selkoe, D.J. *et al.* (2002) Aspartate mutations in presenilin and gamma-secretase inhibitors both impair notch1 proteolysis and nuclear translocation with relative preservation of notch1 signaling. *J. Neurochem.*, **75**, 583–593.
36. Steiner, H. and Haass, C. (2000) Intramembrane proteolysis by presenilins. *Nat. Rev. Mol. Cell Biol.*, **1**, 217–224.
37. Kang, D.E., Soriano, S., Xia, X., Eberhart, C.G., De Strooper, B., Zheng, H. and Koo, E.H. (2002) Presenilin couples the paired phosphorylation of beta-catenin independent of axin: implications for beta-catenin activation in tumorigenesis. *Cell*, **110**, 751–762.
38. Zhang, Z., Hartmann, H., Do, V.M., Abramowski, D., Sturchler-Pierrat, C., Staufenbiel, M., Sommer, B., van de Wetering, M., Clevers, H., Saftig, P. *et al.* (1998) Destabilization of beta-catenin by mutations in presenilin-1 potentiates neuronal apoptosis. *Nature*, **395**, 698–702.
39. Kang, D.E., Soriano, S., Frosch, M.P., Collins, T., Naruse, S., Sisodia, S.S., Leibowitz, G., Levine, F. and Koo, E.H. (1999) Presenilin 1 facilitates the constitutive turnover of beta-catenin: differential activity of Alzheimer's disease-linked PS1 mutants in the beta-catenin-signaling pathway. *J. Neurosci.*, **19**, 4229–4237.
40. Murayama, M., Tanaka, S., Palacino, J., Murayama, O., Honda, T., Sun, X., Yasutake, K., Nihonmatsu, N., Wolozin, B. and Takashima, A. (1998) Direct association of presenilin-1 with beta-catenin. *FEBS Lett.*, **433**, 73–77.
41. Takashima, A., Murayama, M., Murayama, O., Kohno, T., Honda, T., Yasutake, K., Nihonmatsu, N., Mercken, M., Yamaguchi, H., Sugihara, S. *et al.* (1998) Presenilin 1 associates with glycogen synthase kinase-3beta and its substrate tau. *Proc. Natl. Acad. Sci. U. S. A.*, **95**, 9637–9641.
42. Gantier, R., Gilbert, D., Dumanchin, C., Campion, D., Davoust, D., Toma, F. and Frebourg, T. (2000) The pathogenic L392V mutation of presenilin 1 decreases the affinity to glycogen synthase kinase-3 beta. *Neurosci. Lett.*, **283**, 217–220.
43. Prager, K., Wang-Eckhardt, L., Fluhrer, R., Killick, R., Barth, E., Hampel, H., Haass, C. and Walter, J. (2007) A structural switch of presenilin 1 by glycogen synthase kinase 3beta-mediated phosphorylation regulates the interaction with beta-catenin and its nuclear signaling. *J. Biol. Chem.*, **282**, 14083–14093.

44. Hiltunen, M., Helisalmi, S., Mannermaa, A., Alafuzoff, I., Koivisto, A.M., Lehtovirta, M., Pirskanen, M., Sulkava, R., Verkkoniemi, A. and Soininen, H. (2000) Identification of a novel 4.6-kb genomic deletion in presenilin-1 gene which results in exclusion of exon 9 in a Finnish early onset Alzheimer's disease family: an Alu core sequence-stimulated recombination? *Eur. J. Hum. Genet.*, **8**, 259–266.
45. Kasa, P., Papp, H. and Pakaski, M. (2001) Presenilin-1 and its N-terminal and C-terminal fragments are transported in the sciatic nerve of rat. *Brain Res.*, **909**, 159–169.
46. Papp, H., Pakaski, M. and Kasa, P. (2002) Presenilin-1 and the amyloid precursor protein are transported bidirectionally in the sciatic nerve of adult rat. *Neurochem. Int.*, **41**, 429–435.
47. Sheng, J.G., Price, D.L. and Koliatsos, V.E. (2003) The beta-amyloid-related proteins presenilin 1 and BACE1 are axonally transported to nerve terminals in the brain. *Exp. Neurol.*, **184**, 1053–1057.
48. Kamal, A., Almenar-Queralt, A., LeBlanc, J.F., Roberts, E.A. and Goldstein, L.S. (2001) Kinesin-mediated axonal transport of a membrane compartment containing beta-secretase and presenilin-1 requires APP. *Nature*, **414**, 643–648.
49. Gunawardena, S., Yang, G. and Goldstein, L.S. (2013) Presenilin controls kinesin-1 and dynein function during APP-vesicle transport in vivo. *Hum. Mol. Genet.*, **22**, 3828–3843.
50. Weaver, C., Leidel, C., Szpankowski, L., Farley, N.M., Shubeita, G.T. and Goldstein, L.S. (2013) Endogenous GSK-3/shaggy regulates bidirectional axonal transport of the amyloid precursor protein. *Traffic*, **14**, 295–308.
51. Dolma, K., Iacobucci, G.J., Hong Zheng, K., Shandilya, J., Toska, E., White, J.A., II, Spina, E. and Gunawardena, S. (2014) Presenilin influences glycogen synthase kinase-3 beta (GSK-3beta) for kinesin-1 and dynein function during axonal transport. *Hum. Mol. Genet.*, **23**, 1121–1133.
52. Gunawardena, S. and Goldstein, L.S. (2001) Disruption of axonal transport and neuronal viability by amyloid precursor protein mutations in Drosophila. *Neuron*, **32**, 389–401.
53. Morfini, G., Szebenyi, G., Elluru, R., Ratner, N. and Brady, S.T. (2002) Glycogen synthase kinase 3 phosphorylates kinesin light chains and negatively regulates kinesin-based motility. *EMBO J.*, **21**, 281–293.
54. Twomey, C. and McCarthy, J.V. (2006) Presenilin-1 is an unprimed glycogen synthase kinase-3beta substrate. *FEBS Lett.*, **580**, 4015–4020.
55. Uemura, K., Kuzuya, A., Shimozono, Y., Aoyagi, N., Ando, K., Shimohama, S. and Kinoshita, A. (2007) GSK3beta activity modifies the localization and function of presenilin 1. *J. Biol. Chem.*, **282**, 15823–15832.
56. Gindhart, J.G., Jr, Desai, C.J., Beushausen, S., Zinn, K. and Goldstein, L.S. (1998) Kinesin light chains are essential for axonal transport in Drosophila. *J. Cell Biol.*, **141**, 443–454.
57. Hurd, D.D., Stern, M. and Saxton, W.M. (1996) Mutation of the axonal transport motor kinesin enhances paralytic and suppresses Shaker in Drosophila. *Genetics*, **142**, 195–204.
58. Bowman, A.B., Kamal, A., Ritchings, B.W., Philp, A.V., McGrail, M., Gindhart, J.G. and Goldstein, L.S. (2000) Kinesin-dependent axonal transport is mediated by the sunday driver (SYD) protein. *Cell*, **103**, 583–594.
59. Falzone, T.L., Gunawardena, S., McCleary, D., Reis, G.F. and Goldstein, L.S. (2010) Kinesin-1 transport reductions enhance human tau hyperphosphorylation, aggregation and neurodegeneration in animal models of tauopathies. *Hum. Mol. Genet.*, **19**, 4399–4408.
60. Gunawardena, S., Her, L.S., Brusch, R.G., Laymon, R.A., Niesman, I.R., Gordesky-Gold, B., Sintasath, L., Bonini, N.M. and Goldstein, L.S. (2003) Disruption of axonal transport by loss of huntingtin or expression of pathogenic polyQ proteins in Drosophila. *Neuron*, **40**, 25–40.
61. Haghnia, M., Cavalli, V., Shah, S.B., Schimmelpfeng, K., Brusch, R., Yang, G., Herrera, C., Pilling, A. and Goldstein, L.S. (2007) Dynactin is required for coordinated bidirectional motility, but not for dynein membrane attachment. *Mol. Biol. Cell*, **18**, 2081–2089.
62. Horiuchi, D., Collins, C.A., Bhat, P., Barkus, R.V., Diantonio, A. and Saxton, W.M. (2007) Control of a kinesin-cargo linkage mechanism by JNK pathway kinases. *Curr. Biol.*, **17**, 1313–1317.
63. Iacobucci, G.J., Rahman, N.A., Valtuena, A.A., Nayak, T.K. and Gunawardena, S. (2014) Spatial and temporal characteristics of normal and perturbed vesicle transport. *PLoS One*, **9**, e97237.
64. Power, D., Srinivasan, S. and Gunawardena, S. (2012) In-vivo evidence for the disruption of Rab11 vesicle transport by loss of huntingtin. *Neuroreport*, **23**, 970–977.
65. White, J.A., Anderson, E., Zimmerman, K., Zheng, K.H., Rouhani, R. and Gunawardena, S. (2015) Huntingtin differentially regulates the axonal transport of a sub-set of Rab-containing vesicles in vivo. *Hum. Mol. Genet.*, **24**, 7182–7195.
66. Duncan, J.E., Lytle, N.K., Zuniga, A. and Goldstein, L.S. (2013) The microtubule regulatory protein stathmin is required to maintain the integrity of axonal microtubules in Drosophila. *PLoS One*, **8**, e68324.
67. Sisodia, S.S., Kim, S.H. and Thinakaran, G. (1999) Function and dysfunction of the presenilins. *Am. J. Hum. Genet.*, **65**, 7–12.
68. Noll, E., Medina, M., Hartley, D., Zhou, J., Perrimon, N. and Kosik, K.S. (2000) Presenilin affects arm/beta-catenin localization and function in Drosophila. *Dev. Biol.*, **227**, 450–464.
69. Lee, K.D. and Hollenbeck, P.J. (1995) Phosphorylation of kinesin in vivo correlates with organelle association and neurite outgrowth. *J. Biol. Chem.*, **270**, 5600–5605.
70. Gao, F.J., Hebbar, S., Gao, X.A., Alexander, M., Pandey, J.P., Walla, M.D., Cotham, W.E., King, S.J. and Smith, D.S. (2015) GSK-3beta phosphorylation of cytoplasmic dynein reduces Ndel1 binding to intermediate chains and alters dynein motility. *Traffic*, **16**, 941–961.
71. McIlvain, J.M., Jr, Burkhardt, J.K., Hamm-Alvarez, S., Argon, Y. and Sheetz, M.P. (1994) Regulation of kinesin activity by phosphorylation of kinesin-associated proteins. *J. Biol. Chem.*, **269**, 19176–19182.
72. Annaert, W.G., Levesque, L., Craessaerts, K., Dierinck, I., Snellings, G., Westaway, D., George-Hyslop, P.S., Cordell, B., Fraser, P. and De Strooper, B. (1999) Presenilin 1 controls gamma-secretase processing of amyloid precursor protein in pre-golgi compartments of hippocampal neurons. *J. Cell Biol.*, **147**, 277–294.
73. Chyung, J.H., Raper, D.M. and Selkoe, D.J. (2005) Gamma-secretase exists on the plasma membrane as an intact complex that accepts substrates and effects intramembrane cleavage. *J. Biol. Chem.*, **280**, 4383–4392.
74. Bourouis, M. (2002) Targeted increase in shaggy activity levels blockages wingless signaling. *Genesis*, **34**, 99–102.
75. Kirschenbaum, F., Hsu, S.C., Cordell, B. and McCarthy, J.V. (2001) Substitution of a glycogen synthase kinase-3beta phosphorylation site in presenilin 1 separates presenilin function from beta-catenin signaling. *J. Biol. Chem.*, **276**, 7366–7375.

76. McCarthy, J.V. (2005) Involvement of presenilins in cell-survival signalling pathways. *Biochem. Soc. Trans.*, **33**, 568–572.
77. Saura, C.A., Tomita, T., Soriano, S., Takahashi, M., Leem, J.Y., Honda, T., Koo, E.H., Iwatsubo, T. and Thinakaran, G. (2000) The nonconserved hydrophilic loop domain of presenilin (PS) is not required for PS endoproteolysis or enhanced abeta 42 production mediated by familial early onset Alzheimer's disease-linked PS variants. *J. Biol. Chem.*, **275**, 17136–17142.
78. Maesako, M., Horlacher, J., Zoltowska, K.M., Kastanenka, K.V., Kara, E., Svirsky, S., Keller, L.J., Li, X., Hyman, B.T., Bacskai, B.J. and Berezovska, O. (2017) Pathogenic PS1 phosphorylation at Ser367. *Elife*, **6**. Doi: 10.7554/eLife.19720.
79. Wahlster, L., Arimon, M., Nasser-Ghodsi, N., Post, K.L., Serrano-Pozo, A., Uemura, K. and Berezovska, O. (2013) Presenilin-1 adopts pathogenic conformation in normal aging and in sporadic Alzheimer's disease. *Acta Neuropathol.*, **125**, 187–199.
80. Gudkov, A.V., Kazarov, A.R., Thimmapaya, R., Axenovich, S.A., Mazo, I.A. and Roninson, I.B. (1994) Cloning mammalian genes by expression selection of genetic suppressor elements: association of kinesin with drug resistance and cell immortalization. *Proc. Natl. Acad. Sci. U. S. A.*, **91**, 3744–3748.
81. Niclas, J., Navone, F., Hom-Booker, N. and Vale, R.D. (1994) Cloning and localization of a conventional kinesin motor expressed exclusively in neurons. *Neuron*, **12**, 1059–1072.
82. Nakagawa, T., Tanaka, Y., Matsuoka, E., Kondo, S., Okada, Y., Noda, Y., Kanai, Y. and Hirokawa, N. (1997) Identification and classification of 16 new kinesin superfamily (KIF) proteins in mouse genome. *Proc. Natl. Acad. Sci. U. S. A.*, **94**, 9654–9659.
83. Xia, C., Rahman, A., Yang, Z. and Goldstein, L.S. (1998) Chromosomal localization reveals three kinesin heavy chain genes in mouse. *Genomics*, **52**, 209–213.
84. McDonald, A., Fogarty, S., Leclerc, I., Hill, E.V., Hardie, D.G. and Rutter, G.A. (2010) Cell-wide analysis of secretory granule dynamics in three dimensions in living pancreatic beta-cells: evidence against a role for AMPK-dependent phosphorylation of KLC1 at Ser517/Ser520 in glucose-stimulated insulin granule movement. *Biochem. Soc. Trans.*, **38**, 205–208.
85. Hollenbeck, P.J. (1993) Phosphorylation of neuronal kinesin heavy and light chains in vivo. *J. Neurochem.*, **60**, 2265–2275.
86. Schafer, B., Gotz, C., Dudek, J., Hessenauer, A., Matti, U. and Montenarh, M. (2009) KIF5C: a new binding partner for protein kinase CK2 with a preference for the CK2alpha' subunit. *Cell. Mol. Life Sci.*, **66**, 339–349.
87. Verhey, K.J. and Hammond, J.W. (2009) Traffic control: regulation of kinesin motors. *Nat. Rev. Mol. Cell Biol.*, **10**, 765–777.
88. Woźniak, M.J. and Allan, V.J. (2006) Cargo selection by specific kinesin light chain 1 isoforms. *EMBO J.*, **25**, 5457–5468.
89. Verhey, K.J., Meyer, D., Deehan, R., Blenis, J., Schnapp, B.J., Rapoport, T.A. and Margolis, B. (2001) Cargo of kinesin identified as JIP scaffolding proteins and associated signaling molecules. *J. Cell Biol.*, **152**, 959–970.
90. Pigino, G., Morfini, G., Pelsman, A., Mattson, M.P., Brady, S.T. and Busciglio, J. (2003) Alzheimer's presenilin 1 mutations impair kinesin-based axonal transport. *J. Neurosci.*, **23**, 4499–4508.
91. Stokin, G.B., Almenar-Queralt, A., Gunawardena, S., Rodrigues, E.M., Falzone, T., Kim, J., Lillo, C., Mount, S.L., Roberts, E.A., McGowan, E., Williams, D.S. and Goldstein, L.S.B. (2008) Amyloid precursor protein-induced axonopathies are independent of amyloid-beta peptides. *Hum. Mol. Genet.*, **17**, 3474–3486.
92. Fye, S., Dolma, K., Kang, M.J. and Gunawardena, S. (2010) Visualization of larval segmental nerves in 3(rd) instar Drosophila larval preparations. *J. Vis. Exp.*, in press. **43**, pii: 2128. Doi: 10.3791/2128.
93. Day, R.W. and Quinn, G.P. (1989) Comparisons of treatments after an analysis of variance in ecology. *Ecol. Monogr.*, **59**, 433–463.
94. Stewart-Oaten, A. (1995) Rules and judgements in statistics: three examples. *Ecology*, **76**, 2001–2009.